Continuous direct band-gap narrowing and piezochromism of lead-free two-dimensional perovskite nanocrystals under high pressure

Yu Zhou,[1,*] Dianlong Zhao,[1,*] Feng Wang,[1] Yue Shi,[1] Zhiwei Ma,[1] Ruijing Fu,[2,†] Kai Wang,[3] Yongming Sui,[1,‡] Qingfeng Dong,[4] Guanjun Xiao,[1,§] and Bo Zou[1]

[1]*State Key Laboratory of Superhard Materials, College of Physics, Jilin University, Changchun 130012, China*

[2]*College of Applied Physics and Materials, Wuyi University, Jiangmen 529020, China*

[3]*Shandong Key Laboratory of Optical Communication Science and Technology, School of Physics Science and Information Technology, Liaocheng University, Liaocheng 252000, China*

[4]*State Key Laboratory of Supermolecular Structure and Materials, College of Chemistry, Jilin University, Changchun 130012, China*

(Received 17 July 2022; revised 23 May 2023; accepted 7 July 2023; published 26 July 2023)

Lead halide perovskites are widely applied in photovoltaic devices and solar cells. However, the economic potential is restricted by the toxicity of lead. Two-dimensional (2D) layered organic-inorganic hybrid perovskite (OIHP) copper-based perovskites with good stability and hypotoxicity greatly fulfill environmentally favorable standards. Herein, we systematically report a synthesis and band-gap modulation of 2D layered OIHP PEA_2CuCl_4 ($PEA^+ = C_6H_5C_2H_4NH_3$) nanocrystals (NCs). The direct band gap of PEA_2CuCl_4 NCs is effectively decreased from 2.93 to 1.77 eV by using high-pressure technique, accompanied by the piezochromism of products from yellow to dark red and then to opaque black, which enhances the photovoltaic application to a greater extent. Combining experiments and theoretical analysis indicates that direct band-gap narrowing is caused by the shorted average Cl–Cu–Cl bond length, resulting in increased Cu-3*d* and Cl-3*p* interaction, which raises the valence-band maximum toward the conduction-band minimum. The study contributes to a better understanding of 2D layered OIHP PEA_2CuCl_4 NCs and enables pressure processing as a reliable technique for improving materials by design in applications.

DOI: 10.1103/PhysRevMaterials.7.074002

I. INTRODUCTION

In recent decades, lead halide organic-inorganic hybrid perovskites (OIHPs) with large carrier diffusion length, high absorption coefficient, and superior optoelectronic properties have been used in numerous optoelectronic applications, including solar cells, light-emitting diodes, photodetectors and sensors, etc. [1–5]. However, some developments of these materials are restricted by their lead toxicity and chemical instability, which have an impact on their large-scale commercialization, environment, as well as human health [6–13]. With this in mind, it is necessary to develop lead-free and inherent-stability perovskite materials to adapt to commercial markets and environmental requirements. The transition metal of copper (Cu) is a viable alternative for Pb in the formation of Cu-based halide perovskite due to its low toxicity, abundance, and low-dimensional electronic structure [14,15]. Furthermore, due to the mightiness of van der Waals interaction between the capping organic molecules and the hydrophobic property of large organic cations, two-dimensional (2D) OIHPs exhibit high stabilities. PEA_2CuCl_4 ($PEA^+ = C_6H_5C_2H_4NH_3$) nanocrystals (NCs) as a typical 2D layered OIHP with low toxicity have recently evoked considerable attention [16–18]. However, the band gap of perovskites is required in practical photovoltaics to meet the requirements approaching the Shockley-Queisser limit [19–21]. Therefore, the large band gap of 2D OIHP PEA_2CuCl_4 NCs is untoward to be applied in practice. To improve the device performance further, exploring an effective approach is thus extremely desirable to achieve band-gap regulation.

By fine-tuning the electronic configuration in halide perovskites, high pressure, as an independent thermodynamic parameter, can improve optical and electrical performances [22–32]; for example, 2D OIHP $(C_4H_9NH_3)_2(CH_3NH_3)_{n-1}Pb_nI_{3n+1}$ $[(BA)_2(MA)_{n-1}Pb_nI_{3n+1},\ n = 1\text{–}4]$ stabilized under pressure exhibits persistent band-gap narrowing by 8.2% [33,34]. At relatively low pressure, the electronic band of 2D layered perovskite $CsPb_2Br_5$ narrows linearly by 0.03 eV from its initial value of 2.37 eV, which is more robust with respect to external pressure [35]. The study of lead halide OIHP under high pressure has not only realized interesting experimental phenomena but also revealed the relationship between their structure and optical properties, which provides new guidance for the exploration of Cu-based OIHP.

Herein, we have designed a facile synthetic strategy for 2D OIHP PEA_2CuCl_4 NCs and realized the band-gap narrowing to approximately 1.77 eV under high pressure. The small band gap caused by absorption redshift is promising in lead-free 2D OIHP. Meanwhile, *in situ* high-pressure

*These authors contributed equally to this work.
†ruijingfu_wyu@163.com
‡suiym@jlu.edu.cn
§xguanjun@jlu.edu.cn

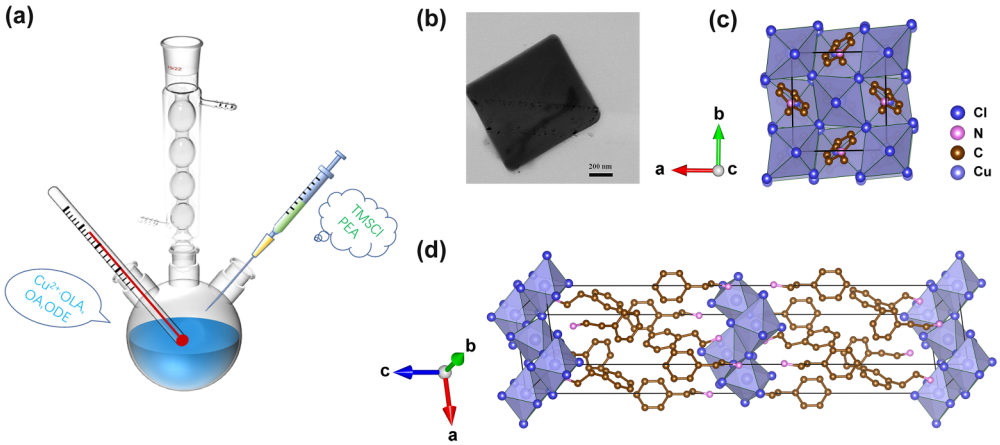

FIG. 1. (a) Schematic illustration for the synthesis of PEA_2CuCl_4 NCs. (b) TEM image of PEA_2CuCl_4 NCs. (c) Crystal structure viewed in *ab* plane of PEA_2CuCl_4 NCs. (d) Two-dimensional layered PEA_2CuCl_4 NCs. N, C, Cu, and Cl atoms are shown as pink, brown, purple, and blue spheres, respectively.

measurements were conducted to establish comprehensive studies related to pressure response, which also included angular dispersive x-ray diffraction spectra (ADXRD), Raman spectra, and absorption spectra. In addition, pressure-triggered tunable absorption with a 1.16-eV redshift was attributed to the structural compression behavior in 2D OIHP PEA_2CuCl_4 NCs. Correlating with *in situ* ADXRD, Raman spectra, and first-principles calculations, we effectively investigated the relationship between band-gap properties and the structure of PEA_2CuCl_4 NCs due to the unique 2D structure, which enables the organic layer to be compressed first. Moreover, first-principles calculations further clarify that the shorted average Cl–Cu–Cl bond length resulted in increased Cu-3*d* and Cl-3*p* interaction, which raises the valence-band maximum (VBM) toward the conduction-band minimum (CBM), leading to reduction of band gap. The issue independently designed an effective approach to synthesizing lead-free 2D OIHP PEA_2CuCl_4 NCs by drawing on the synthesis methods of other substances. Moreover, it provided insights into the structure-property relationship in lead-free 2D OIHPs.

II. RESULTS AND DISCUSSION

The synthesis of OIHP PEA_2CuCl_4 NCs was performed using a hot-injection approach [Fig. 1(a); details in Supplemental Material] [36]. Transmission electron microscopy (TEM) was used to examine the morphology and structure of the synthesized PEA_2CuCl_4 NCs. As shown in Fig. 1(b), the samples exhibit a nanocube morphology with a dimension of 700 nm before compression. The structure consists of a Cu-*X* octahedral network formed by the stacking of inorganic layers alternating with organic sheets of PEA^+ cations [Figs. 1(c) and 1(d)] [37] (see the Supplemental Material reference [1] in [37]). Alkylammonium organic cations are more flexible, and the unique 2D layer organic-inorganic metal halide has greater spatial flexibility and compressibility [Figs. S1(a) and S1(b)] [36], resulting in novel optical properties under high pressure.

Based on the Shockley-Queisser model, it is known that a perfect band gap is essential for high-performance optoelectronic materials. Regretfully, large band gaps are typically displayed in layered perovskites leading to undesirable power-conversion efficiency limits [38]. Therefore, we expect to regulate the band gap through high pressure to obtain a more appropriate band-gap value. Meanwhile, we investigated PEA_2CuCl_4 NCs by *in situ* high-pressure absorption experiment, in which silicone oil was used as the pressure-transfer medium, and ruby spheres were used for pressure calibration [39] (see the Supplemental Material reference [2] in [39]). As shown in Fig. 2(a), the absorption edge distinctly exhibited a steep exciton edge. As the pressure increased, the PEA_2CuCl_4

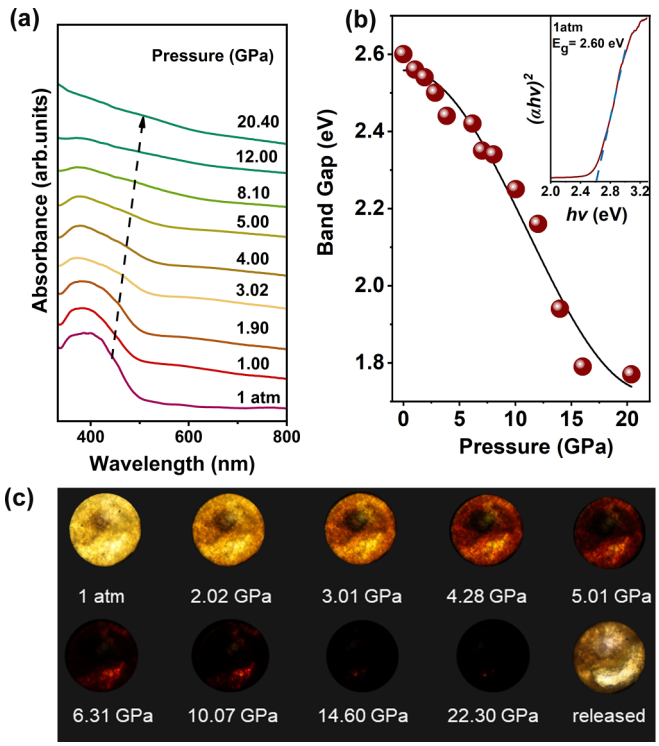

FIG. 2. (a) Absorption spectra of PEA_2CuCl_4 NCs under high pressure. (b) Band-gap evolution of PEA_2CuCl_4 NCs upon compression. Inset shows Tauc plot for PEA_2CuCl_4 NCs at 1 atm. (c) Optical micrograph of PEA_2CuCl_4 NCs in diamond-anvil cell under high pressure.

NCs maintained a relatively clear absorption edge before 4.0 GPa, and a slight redshift was accompanied by a 0.2-eV reduction in the band gap [Fig. 2(b)]. However, the absorption edge became increasingly widened and finally disappeared at higher pressure, which may relate to the change of structure and electronic landscape of the sample. The band gap of PEA_2CuCl_4 NCs under different pressures by extrapolating the linear portion of $(\alpha h\nu)^2$ versus the $h\nu$ curve [Fig. 2(b)] was analyzed (α is the absorption coefficient and $h\nu$ is the photon energy). In Fig. S2, the band gap is continuously narrowed from 2.93 to 1.77 eV, which enables the tunability of the band gap of PEA_2CuCl_4 NCs. To heighten the accuracy of the test results, the UV-Vis absorption experiment was repeated (Fig. S3) [36]. The experimental results were consistent with the previous ones [Fig. 2(a)]. Meanwhile, the absorption edge was not fully recovered when pressure was returned to ambient pressure [Figs. S4(a) and S4(b)] [36]. In addition, interesting piezoceramics were achieved in PEA_2CuCl_4 NCs as shown in Fig. 2(c) [40]. When the pressure reached 3.01 GPa, the variation occurred from translucent yellow to red. Upon further compression, the color of the substance was changed from translucent red to opaque black at about 10.07 GPa, which is well in agreement with the evaluation of the band gap under high pressure.

In situ high-pressure ADXRD experiment was performed to further assess the connection between the structure and optical properties of PEA_2CuCl_4 NCs. In the integrated spectra as shown in Fig. 3(a), it was found that there are no new XRD peaks generated during the pressurization process except for the Bragg diffraction peak moving to higher diffraction angles, which indicates compression occurring for crystal structure of PEA_2CuCl_4 NCs before 5.2 GPa. Upon further compression to 8.3 GPa, some of the diffraction peaks gradually broadened and weakened, indicating that the structure was deformed to a greater extent under higher pressure. Finally, the Bragg diffraction peaks entirely disappeared, and only faint broadband remained once the pressure reached 22.30 GPa, which indicates that the material was completely amorphized. Part of the amorphous phase began to recrystallize and part of the diffraction peak did not return to the original state upon releasing pressure [Fig. S4(c)] [36].

To get insights into the structural evolution under high pressure, the crystal structure of PEA_2CuCl_4 NCs was refined. The *R* factors (unweighted profile *R* factor R_{wp} and weighted profile *R* factor R_p) obtained from the refinement are exhibited in Table SI [36]. The cell parameters and cell volume of PEA_2CuCl_4 NCs were calculated, as shown in Figs. 3(b) and 3(c). It was obviously seen that the lattice constant *c* was more sensitive to pressure than the lattice constants *a* and *b*, indicating a reduction of the cell volume of PEA_2CuCl_4 NCs mainly resulting from *c*-axis compression. PEA_2CuCl_4 NCs were an orthorhombic system with the space group *Pbca* ($a = 7.16045$ Å, $b = 7.33469$ Å, and $c = 38.5093$ Å) at ambient pressure [Fig. 3(d)].

To better understand the relationship between structure and optical properties, we performed first-principles computation. We determined the crystal structures at higher pressures using a completely relaxed crystal structure, including both relaxation of atomic positions and lattice parameters, through total energy minimization with the residual forces on the atoms

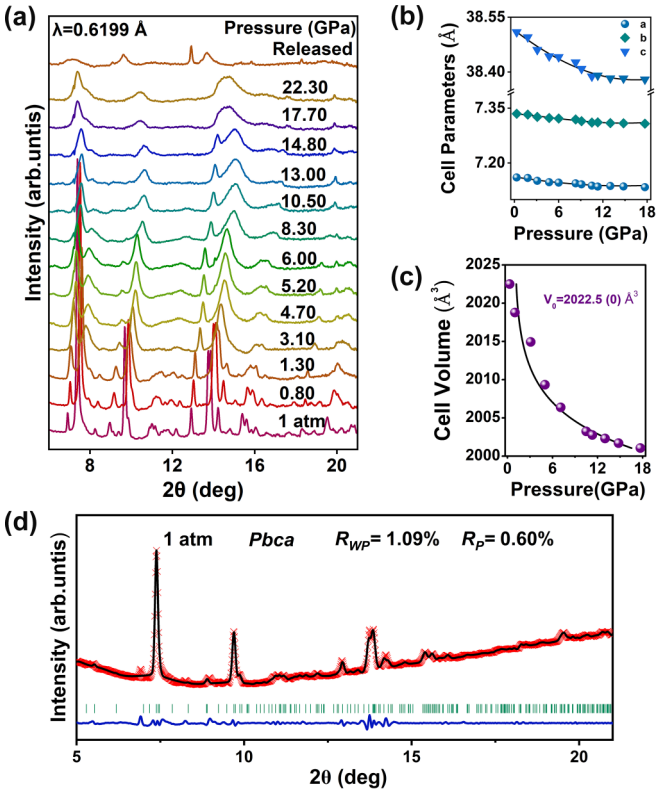

FIG. 3. (a)–(c) High-pressure evolution of ADXRD patterns, cell parameters, and unit-cell volume. (d) Refinement of ADXRD pattern collected at 1 atm. Green lines reflect refined peak positions, and blue line represents differences between experimented (black) and simulated (red) profiles.

converged to below 0.01 eV/Å. Meanwhile, considering the van der Waals interaction in this 2D layer structure optB86b, optB88 and DFT-D2/D3 [optB86b: o-p-t-B-8-6-b (stands for Optimized Becke 86 exchange with the B parameter); optB88: o-p-t-B-8-8 (stands for Optimized Becke 88 exchange) DFT-D2/D3: D-F-T-D-2-slash-D-3 (stands for Density Functional Theory with D2 or D3 dispersion corrections)] method of Grimme were tested to optimize the structure. We found that the calculated lattice parameters of theoretical calculation are well in agreement with the experimental value by employing DFT-D3 method of Grimme, as shown in Table SII [36]. In addition, spin-orbit coupling (SOC) is not important in this material and thus we can neglect it (Fig. S5) [36,40,41]. As shown in Fig. 4(a), the PEA_2CuCl_4 exhibited a direct band gap at Γ points under ambient conditions. Partial density of states (DOS) shows that the Cu 3*d* and Cl 3*p* interactions dominate the VBM of the PEA_2CuCl_4 NCs, while the Cu 3*s* and Cu 3*p* interactions contribute to the CBM [Fig. 4(b)]. Figure 4(c) depicts the evolution trend of pressure-dependent band gap obtained by calculation, which is well in agreement with experimental evolution. Note that PEA_2CuCl_4 NCs exhibit feature of direct band-gap evolution under high pressure (Fig. S6) [36], further facilitating its application in photovoltaic behavior [42]. Furthermore, we investigated the nature of gap evolution. Under ambient conditions, the bond length L2 is much longer than L1 and L3, indicating a severe distortion of the octahedron. Intriguingly, the length

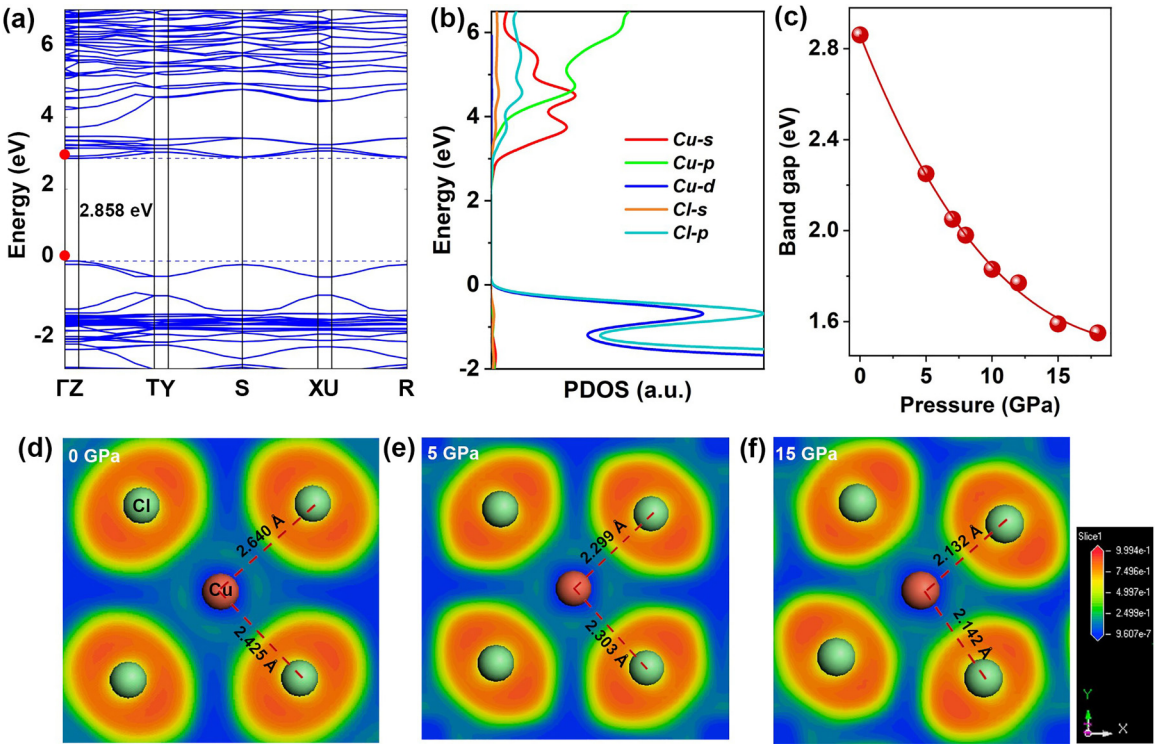

FIG. 4. (a) Calculated electronic band structure of PEA_2CuCl_4 at 1 atm. High-symmetry k path was represented by G (0, 0, 0), Z (0, 0, 0.5)$-T$ (−0.5, 0, 0.5)$-Y$ (−0.5, 0, 0)$-S$ (−0.5, 0.5, 0)$-X$ (0, 0.5, 0)$-U$ (0, 0.5, 0.5)$-R$ (−0.5, 0.5, 0.5) in Brillouin zones. (b) Density of states projected onto Cu and Cl atoms. Inset shows DOS of Cl-p. (c) Calculated band-gap evolution of PEA_2CuCl_4 NCs upon compression. (d)–(f) Calculated ELF in ab plane under high pressure. Dashed lines represent atomic distance of Cu-Cl.

difference of the Cu–Cl bond decreases gradually because of the increased L1 (along the c direction) before 5 GPa, and then L1, L2, and L3 start to decrease [Fig. S7(a)] [36]. Meanwhile, organic layer distance also decreases under high pressure, indicating vertical compression without slip [Fig. S7(b)] [36]. In addition, the average Cu–Cl bond length decreases with increasing pressure, demonstrating global positive compression [Fig. S8(a)] [36]. In addition, before 5 GPa, the standard deviation gradually decreases, indicating distortion of the octahedron decrease, while standard deviation gradually increases with increasing pressure, indicating that $[CuCl_4]^{2-}$ inorganic octahedron was gradually distorted and deformed at higher pressure. Therefore, in the process of increasing pressure, distortion of the octahedron experienced the decrease and increase [Fig. S8(b)] [36]. In addition, the decrease of the average Cl–Cu–Cl bond length results in increased orbital overlap, which is in excellent agreement with the calculated electron local function (ELF) [Figs. 4(d)–4(f)]. Therefore, direct band-gap narrowing is caused by the shorted average Cl–Cu–Cl bond length, resulting in increased Cu-3d and Cl-3p interaction. The schematic illustration of the Cu–Cl bond length in the $[CuCl_4]^{2-}$ framework under compression is shown in Fig. S9 [36].

The interaction between organic and inorganic layers under high pressure was investigated by *in situ* high-pressure Raman spectra at room temperature. In the low frequency, three Raman modes correspond to Cu-Cl vibrations (Fig. S10) at around 170, 251, and 270 cm^{-1} [36], agreeing with the previously reported Raman peaks of $(C_2H_5NH_3)_2[CuCl_4]$ [43]. The frequency shift of the corresponding typical Raman modes of copper chloride as a function of pressure was reported by Li *et al.* [44]. Evidently, three peaks at around 480, 500, and 1000 cm^{-1} correspond to PEA^+ cations, as shown in Figs. S10(a) and S10(b) [36]. During the process of pressurization starting from ambient pressure, a weak band shift to higher frequency of the Cu-Cl vibration occurred due to the lattice contraction, which may be attributed to a decrease in the interatomic distance. When the pressure was raised to around 2.0 GPa, the vibration peaks of the PEA^+ cation disappeared, while the Cu-Cl vibration peaks remained in this process. Moreover, the three peaks were gradually weakened and broadened until they disappeared, indicating that the electronic structure of PEA_2CuCl_4 NCs was enormously changed and that the organic layer was first distorted during the process of pressurization. This fact shows that enough space for the $[CuCl_4]^{2-}$ inorganic octahedron was provided. Moreover, the Cu-Cl vibrations completely disappeared at about 13.0 GPa, manifesting that the $[CuCl_4]^{2-}$ inorganic octahedron was gradually distorted and deformed at higher pressure. The vibrational peaks reappeared upon decompression, with the color from opaque black back to translucent yellow.

III. CONCLUSION

We successfully synthesized 2D OIHP PEA_2CuCl_4 NCs by a facie hot-injection method. Note that 2D OIHP PEA_2CuCl_4 NCs exhibit feature of direct band-gap

evolution under high pressure, further facilitating its application in photovoltaic behavior. Importantly, the direct band gap was effectively controlled by high pressure from 2.93 to 1.77 eV, which approaches the Shockley-Queisser limit of photovoltaic applications, accompanied by the piezochromism of products from yellow to dark red and then to opaque black. *In situ* high-pressure experiments and theoretical calculations indicated that such band-gap narrowing was ascribed to the unique 2D layered structure change under high pressure. Therein, the direct band-gap narrowing caused the shorted average Cl–Cu–Cl bond length, resulting in increased Cu − 3*d* and Cl − 3*p* interaction, which raised the VBM toward the CBM. The study contributes to a better understanding of 2D layered OIHP PEA_2CuCl_4 NCs and enables pressure processing as a reliable technique for improving materials by design in applications.

ACKNOWLEDGMENTS

This work is supported by the National Key R&D Program of China (Grant No. 2019YFE0120300), the Fundamental Research Funds for the Central Universities, the National Science Foundation of China (Grants No. 12174144 and No. 12174146), the Special Construction Project Fund for Shandong Province Taishan Scholars, Jilin Provincial Science & Technology Development Program (Grant No. 20220101002JC), and the Science Foundation for High-level Talents of Wuyi University (Grant No. 2021AL019). This work was mainly performed at BL15U1 at the Shanghai Synchrotron Radiation Facility (SSRF). Portions of this work were performed at 4W2HP-Station, Beijing Synchrotron Radiation Facility (BSRF).

[1] L. Xie, B. Chen, F. Zhang, Z. Zhao, X. Wang, L. Shi, Y. Liu, L. Huang, R. Liu, B. Zou *et al.*, Highly luminescent and stable lead-free cesium copper halide perovskite powders for uv-pumped phosphor-converted light-emitting diodes, Photonics Res. **8**, 768 (2020).

[2] P. Pandey, N. Sharma, R. A. Panchal, S. W. Gosavi, and S. Ogale, Realization of high capacity and cycling stability in Pb-Free A_2CuBr_4 ($A = CH_3NH_3/Cs$, 2 D/3 D) perovskite-based Li-Ion battery anodes, ChemSusChem **12**, 3742 (2019).

[3] Y. Liu, B. Dong, A. Hagfeldt, J. Luo, and M. Graetzel, Chemically tailored molecular surface modifiers for efficient and stable perovskite photovoltaics, SmartMat **2**, 33 (2021).

[4] S. Das, S. Gholipour, and M. Saliba, Perovskites for laser and detector applications, Energy Environ. Mater. **2**, 146 (2019).

[5] Z. Xuan, J. Li, Q. Liu, F. Yi, S. Wang, and W. Lu, Artificial structural colors and applications, The Innovation **2**, 100081 (2021).

[6] Z. Yuan, C. Zhou, Y. Tian, Y. Shu, J. Messier, J. C. Wang, L. J. van de Burgt, K. Kountouriotis, Y. Xin, E. Holt *et al.*, One-dimensional organic lead halide perovskites with efficient bluish white-light emission, Nat. Commun. **8**, 14051 (2017).

[7] W. Li, Z. Wang, F. Deschler, S. Gao, R. H. Friend, and A. K. Cheetham, Chemically diverse and multifunctional hybrid organic–inorganic perovskites, Nat. Rev. Mater. **2**, 16099 (2017).

[8] G. Xiao, Y. Cao, G. Qi, L. Wang, C. Liu, Z. Ma, X. Yang, Y. Sui, W. Zheng, and B. Zou, Pressure effects on structure and optical properties in cesium lead bromide perovskite nanocrystals, J. Am. Chem. Soc. **139**, 10087 (2017).

[9] Y. Shi, Z. Ma, D. Zhao, Y. Chen, Y. Cao, K. Wang, G. Xiao, and B. Zou, Pressure-induced emission (PIE) of one-dimensional organic tin bromide perovskites, J. Am. Chem. Soc. **141**, 6504 (2019).

[10] Y. Fang, T. Shao, L. Zhang, L. Sui, G. Wu, K. Yuan, K. Wang, and B. Zou, Harvesting high-quality white-light emitting and remarkable emission enhancement in one-dimensional halide perovskites upon compression, JACS Au **1**, 459 (2021).

[11] Y. Shi, W. Zhao, Z. Ma, G. Xiao, and B. Zou, Self-trapped exciton emission and piezochromism in conventional 3D lead bromide perovskite nanocrystals under high pressure, Chem. Sci. **12**, 14711 (2021).

[12] R. Fu, W. Zhao, L. Wang, Z. Ma, G. Xiao, and B. Zou, Pressure-induced emission toward harvesting cold white light from warm white light, Angew. Chem. Int. Ed. **60**, 10082 (2021).

[13] S. Liu, S. Sun, C. K. Gan, A. G. del Águila, Y. Fang, J. Xing, T. T. H. Do, T. J. White, H. Li, W. Huang *et al.*, Manipulating efficient light emission in two-dimensional perovskite crystals by pressure-induced anisotropic deformation, Sci. Adv. **5**, eaav9445 (2019).

[14] Q. Li, Z. Chen, B. Yang, L. Tan, B. Xu, J. Han, Y. Zhao, J. Tang, and Z. Quan, Pressure-induced remarkable enhancement of self-trapped exciton emission in one-dimensional $CsCu_2I_3$ with tetrahedral units, J. Am. Chem. Soc. **142**, 1786 (2020).

[15] S. Gupta, T. Pandey, and A. K. Singh, Suppression of Jahn–Teller distortions and origin of piezochromism and thermochromism in Cu–Cl hybrid perovskite, Inorg. Chem. **55**, 6817 (2016).

[16] G. Feng, Y. Qin, C. Ran, L. Ji, L. Dong, and W. Li, Structural evolution and photoluminescence properties of a 2D hybrid perovskite under pressure, APL Mater. **6**, 114201 (2018).

[17] L. Zhang, L. Wu, K. Wang, and B. Zou, Pressure-induced broadband emission of 2D organic–inorganic hybrid perovskite $(C_6H_5C_2H_4NH_3)_2PbBr_4$, Adv. Sci. **6**, 1801628 (2019).

[18] J. Qu, S. Xu, F. Liu, Z. Wang, H. Shao, Y. Cui, and C. Wang, Lead-free P-type $Mn:Cs_3Cu_2I_5$ perovskite with tunable dual-color emission through room-temperature grinding method, J. Mater. Sci. **56**, 12326 (2021).

[19] L. Tao, J. Qiu, B. Sun, X. Wang, X. Ran, L. Song, W. Shi, Q. Zhong, P. Li, H. Zhang *et al.*, Stability of mixed-halide wide bandgap perovskite solar cells: Strategies and progress, J. Energy Chem. **61**, 395 (2021).

[20] M. Li, C. Zuo, J. Hu, and L. Ding, Carrier management makes perovskite solar cells approaching Shockley-Queisser limit, Sci. Bull. **66**, 1372 (2021).

[21] B. Ehrler, E. Alarcón-Lladó, S. W. Tabernig, T. Veeken, E. C. Garnett, and A. Polman, Photovoltaics reaching for the Shockley–Queisser limit, ACS Energy Lett. **5**, 3029 (2020).

[22] Y. Fang, L. Zhang, Y. Yu, X. Yang, K. Wang, and B. Zou, Manipulating emission enhancement and piezochromism in two-dimensional organic-inorganic halide perovskite

[(HO)$(CH_2)_2NH_3)]_2PbI_4$ by high pressure, CCS Chem. **3**, 2203 (2020).

[23] L. Wang, K. Wang, G. Xiao, Q. Zeng, and B. Zou, Pressure-induced structural evolution and band gap shifts of organometal halide perovskite-based methylammonium lead chloride, J. Phys. Chem. Lett. **7**, 5273 (2016).

[24] Y. Nagaoka, K. Hills-Kimball, R. Tan, R. Li, Z. Wang, and O. Chen, Nanocube superlattices of cesium lead bromide perovskites and pressure-induced phase transformations at atomic and mesoscale levels, Adv. Mater. **29**, 1606666 (2017).

[25] Z. Ma, F. Li, L. Sui, Y. Shi, R. Fu, K. Yuan, G. Xiao, and B. Zou, Tunable color temperatures and emission enhancement in 1D halide perovskites under high pressure, Adv. Opt. Mater. **8**, 2000713 (2020).

[26] S. Guo, Y. Zhao, K. Bu, Y. Fu, H. Luo, M. Chen, M. P. Hautzinger, Y. Wang, S. Jin, W. Yang *et al.*, Pressure-suppressed carrier trapping leads to enhanced emission in two-dimensional perovskite $(HA)_2(GA)Pb_2I_7$, Angew. Chem. Int. Ed. **59**, 17533 (2020).

[27] Q. Li, Z. Chen, M. Li, B. Xu, J. Han, Z. Luo, L. Tan, Z. Xia, and Z. Quan, Pressure-engineered photoluminescence tuning in zero-dimensional lead bromide trimer clusters, Angew. Chem. Int. Ed. **60**, 2583 (2021).

[28] Z. Ma, G. Xiao, and L. Ding, Pressure-induced emission from low-dimensional perovskites, J. Semicond. **42**, 100203 (2021).

[29] Z. Ma, F. Li, D. Zhao, G. Xiao, and B. Zou, Whether or not emission of Cs_4PbBr_6 nanocrystals: High-pressure experimental evidence, CCS Chem. **2**, 71 (2020).

[30] Z. Ma, Q. Li, J. Luo, S. Li, L. Sui, D. Zhao, K. Yuan, G. Xiao, J. Tang, Z. Quan *et al.*, Pressure-driven reverse intersystem crossing: New path toward bright deep-blue emission of lead-free halide double perovskites, J. Am. Chem. Soc. **143**, 15176 (2021).

[31] D. Zhao, G. Xiao, Z. Liu, L. Sui, K. Yuan, Z. Ma, and B. Zou, Harvesting cool daylight in hybrid organic-inorganic halides microtubules through the reservation of pressure-induced emission, Adv. Mater. **33**, 2100323 (2021).

[32] L. Zhang, C. Liu, L. Wang, C. Liu, K. Wang, and B. Zou, Pressure-induced emission enhancement, band-gap narrowing, and metallization of halide perovskite $Cs_3Bi_2I_9$, Angew. Chem. Int. Ed. **57**, 11213 (2018).

[33] G. Liu, J. Gong, L. Kong, R. D. Schaller, Q. Hu, Z. Liu, S. Yan, W. Yang, C. C. Stoumpos, M. G. Kanatzidis *et al.*, Isothermal pressure-derived metastable states in 2D hybrid perovskites showing enduring bandgap narrowing, Proc. Natl. Acad. Sci. USA. **115**, 8076 (2018).

[34] L. Kong, G. Liu, J. Gong, L. Mao, M. Chen, Q. Hu, X. Lü, W. Yang, M. G. Kanatzidis, and H.-k. Mao, Highly tunable properties in pressure-treated two-dimensional dion–jacobson perovskites, Proc. Natl. Acad. Sci. USA. **117**, 16121 (2020).

[35] Z. Ma, F. Li, G. Qi, L. Wang, C. Liu, K. Wang, G. Xiao, and B. Zou, Structural stability and optical properties of two-dimensional perovskite-like $CsPb_2Br_5$ microplates in response to pressure, Nanoscale **11**, 820 (2019).

[36] See Supplemental Material at http://link.aps.org/supplemental/10.1103/PhysRevMaterials.7.074002 for the details of synthesis and additional figures and tables in support of the data analysis.

[37] R. D. Willett, Structures of the antiferrodistortive layer perovskites bis(phenethylammonium) tetrahalocuprate(II), Halo = Cl^-, Br^-, Acta Cryst. **C46**, 565 (1990).

[38] S. Kim and A. Walsh, Ab initio calculation of the detailed balance limit to the photovoltaic efficiency of single p-n junction kesterite solar cells, Appl. Phys. Lett. **118**, 243905 (2021).

[39] H. K. Mao, J. Xu, and P. M. Bell, Calibration of the ruby pressure gauge to 800 kbar under quasi-hydrostatic conditions, J. Geophys. Res. **91**, 4673 (1986).

[40] L. Wang, P. Yao, F. Wang, S. Li, Y. Chen, T. Xia, E. Guo, K. Wang, B. Zou, and H. Guo, Pressure-induced structural evolution and bandgap optimization of lead-free halide double perovskite $(NH_4)_2SeBr_6$, Adv. Sci. **7**, 1902900 (2020).

[41] T. Das, G. Di Liberto, and G. Pacchioni, Density functional theory estimate of halide perovskite band gap: When spin orbit coupling helps, J. Phys. Chem. C. **126**, 2184 (2022).

[42] G. Di Liberto, O. Fatale, and G. Pacchioni, Role of surface termination and quantum size in α-$CsPbX_3$ (X = Cl, Br, I) 2D nanostructures for solar light harvesting, Phys. Chem. Chem. Phys. **23**, 3031 (2021).

[43] A. Jaffe, Y. Lin, W. L. Mao, and H. I. Karunadasa, Pressure-induced conductivity and yellow-to-black piezochromism in a layered Cu–Cl hybrid perovskite, J. Am. Chem. Soc. **137**, 1673 (2015).

[44] Q. Li, S. Li, K. Wang, Z. Quan, Y. Meng, and B. Zou, High-pressure study of perovskite-like organometal halide: Band-gap narrowing and structural evolution of $[NH_3\text{-}(CH_2)_4\text{-}NH_3]CuCl_4$, J. Phys. Chem. Lett. **8**, 500 (2017).